Fabrication, dynamics, and electrical properties of insulated scanning probe microscopy probes for electrical and electromechanical imaging in liquids

B. J. Rodriguez, S. Jesse, K. Seal, A. P. Baddorf, and S. V. Kalinin[a),b)]
Oak Ridge National Laboratory, Oak Ridge, Tennessee 37831

P. D. Rack[a),c)]
Oak Ridge National Laboratory, Oak Ridge, Tennessee 37831, and Department of Materials Science and Engineering, University of Tennessee, Knoxville, Tennessee 37996

(Received 19 July 2007; accepted 10 August 2007; published online 30 August 2007)

Insulated cantilever probes with a high aspect ratio conducting apex have been fabricated and their dynamic and electrical properties analyzed. The cantilevers were coated with silicon dioxide and a via was fabricated through the oxide at the tip apex and backfilled with tungsten to create an insulated probe with a conducting tip. The stiffness and Q factor of the cantilevers increased after the modifications and their resonances shifted to higher frequencies. The coupling strength between the cantilever and the coating are determined. Electromechanical imaging of ferroelectric domains, current voltage probing of a gold surface, and a probe apex repair process are demonstrated. © *2007 American Institute of Physics*. [DOI: 10.1063/1.2778762]

The ubiquity of electromechanical phenomena in biological and biomolecular systems ranging from voltage controlled muscular contractions[1] to cell electromotility,[2] ion channels, and electromotor proteins[3] necessitates probing of these phenomena on the tissue, cellular, subcellular, and molecular levels. Scanning probe microscopy (SPM) studies of biological systems necessitate the use of a liquid environment to maintain a native environment for biomolecules and cells to control tip-surface forces and to eliminate capillary interactions. For electromechanical measurements, an additional degree of complexity is introduced by the conductivity of the liquid medium, resulting in stray currents and electrochemical reactions, thus precluding precise control of dc and ac probe potentials.

The use of high (0.1–25 MHz) imaging frequencies combined with direct or frequency-mixing detection allows one to avoid electrochemical processes for piezoelectric[4] and dielectroforetic force[5] imaging. However, the large response times (~0.1–10 ms) of biological systems, combined with the requirement for precise control of local electrochemical potentials, require dc potential localization in solution within the probed volume. By using model ferroelectric systems and conventional metal-coated probes, it was shown that the electric field can be localized only in weakly conductive solvents such as isopropanol,[6] whereas even distilled water results in a delocalized dc field. These considerations necessitate the development of insulated SPM probes,[7–9] which effectively combine probe microscopy and patch-clamp techniques.[1]

The application of insulating coated probes to electromechanical and electrical probings in liquid environments requires (a) good dynamic properties and reflectivity of the lever, (b) good insulation except for the apex, (c) high apex conductivity, and (d) an apex geometry consistent with high resolution. In this letter, we describe a process for fabricating shielded probes, the effect of the coating on the dynamic and electrical properties, and the operation in conductive and electromechanical imaging modes in ambient and liquid environments.

Commercial doped-Si atomic force microscope (AFM) cantilevers [tip 1: RFESP (Veeco) and tip 2: AC240TS (Olympus)] were initially coated on both sides with ~500 nm silicon oxide by a plasma enhanced chemical vapor deposition (PECVD) process. The specific processing parameters were 350 °C, 85 SCCM (SCCM denotes cubic centimeter per minute at STP) Ar(95%)–SiH_4(5%), and 157 SCCM N_2O, and a total processing pressure of 1 Torr, 20 W radio-frequency power, for 7 min in an Oxford PECVD system. To allow for electrical contact, Kapton tape was placed over ~2 mm at the back side of the chip during oxide growth. Subsequent AFM tip processing was performed in an FEI Nova 600 dual beam scanning electron microscope (SEM)/focused ion beam (FIB). To etch a via through the insulating oxide to the underlying silicon tip, a 100 nm diameter circle pattern was FIB milled into the AFM tip using a 30 keV and 30 pA gallium ion beam for 25 s. The resulting diameters were ~315 nm for tip 1 and ~240 nm for tip 2. SEM images of tip 1 and tip 2 after the oxide deposition and after the via FIB are shown in Figs. 1(a), 1(b), 1(d), and 1(e), respectively. Some peripheral etch damage is observed in tip 1 which occurred during acquisition of an ion beam image. Subsequent to the via etch, a "tungsten" contact was deposited in the via using electron beam induced deposition (EBID).[10] A 10 keV (20 pA) electron beam in spot mode was used and the deposition precursor was $W(CO)_6$. Tip 1 was deposited for 35 s and tip 2 was deposited for 20 s. Typical EBID structures deposited from the $W(CO)_6$ precursor are ~ 55 at. % W, 30% C and 15% O.[11] SEM images of tip 1 and tip 2 after the EBID fill are shown in Figs. 1(c) and 1(f), respectively.

Dynamic characteristics of the cantilever, tip-surface contact resistance, and piezoresponse force microscopy

[a)]Authors to whom correspondence should be addressed.
[b)]Electronic mail: sergei2@ornl.gov
[c)]Electronic mail: prack@utk.edu

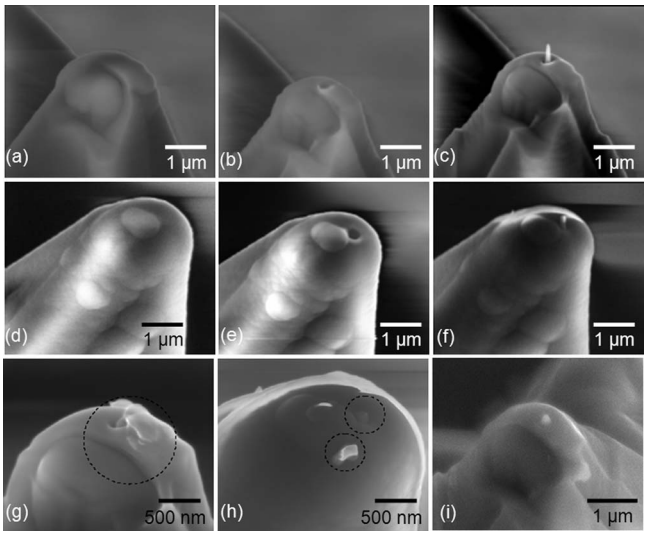

FIG. 1. SEM images [(a) and (d)] after the oxide deposition, [(b) and (e)] after the via FIB, and [(c) and (f)] after the EBID fill for tip 1 and tip 2, respectively. [(g) and (h)] SEM images of tip 1 and tip 2, respectively, after using the tips for contact mode imaging. (i) SEM of tip 1 after repairing the plug in (g). Circles in (g) and (h) show the damaged plugs.

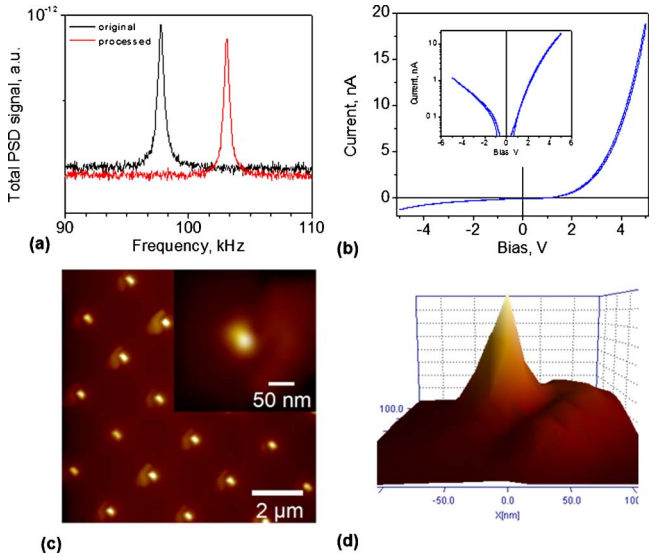

FIG. 2. (Color online) (a) First thermal resonance before and after the tip processing for tip 1, (b) *I-V* curve for tip 1 (repaired), (c) scan of calibration grating using tip 1 (repaired) with the inset of tip reconstruction (z scale is 162.5 nm), and (d) three-dimensional representation of tip shape. The z scale for (c) is 200 nm.

(PFM) imaging in ambient and liquid environments were measured using an Asylum Research MFP-3D AFM with an additional function generator and lock-in amplifier (DS 345 and SRS 844, Stanford Research Systems). The scanner head was modified to allow direct access to the tip deflection signals. Before and after the processing, the photodetector sum signal, force-distance curves, and thermal tunes were measured and recorded. The contact resistance and current-voltage (*I-V*) curves were measured on a clean Au(111) surface. The PFM imaging[12] was performed using a periodically poled lithium niobate (PPLN) crystal as a model system.

The tips were calibrated before and after processing using established methods to obtain spring constants, Q factor, and inverse optical lever sensitivity (InvOLS) (Table I).[13–15] The first thermal resonance before and after processing for tip 1 is shown in Fig. 2(a) and demonstrates a shift in the first free resonance cantilever to higher frequencies. Note that SiO_2 deposition does not affect the reflectivity of the lever. The spring constant k and resonance frequency of the cantilever are increased. This behavior can easily be understood given that a rectangular cantilever spring constant is related to the geometric parameters of the cantilever as $k=3EI/L^3=Ewh^3/4L^3$, where EI is the product of the Young modulus and the moment of inertia, and L and h are the length and thickness of the cantilever. The resonant frequencies are $\omega_n^2=k\beta_n^4/3m$, where m is the cantilever mass and β_n is the root of the characteristic equation. For a free cantilever, the first three resonances occur at $\beta_n=1.875, 4.694, 7.855$ (compared to $\beta_n=3.927, 7.067, 10.21$ in contact).[16–18]

From the data in Table I, the increase in effective mass for tip 1 is 22.9% and for 55% for tip 2. From the known densities of Si and SiO_2 (2.33 and 2.2 g/cm^3, respectively), the increases in thickness are 24.2% and 58.2%, respectively. For the compound beam formed by a central beam of width w_1 and thickness h_1 surrounded by an external shell of width w_2 and thickness h_2, the effective stiffness is

$$12EI = E_1 h_1^3 w_1 + \alpha E_2 (h_2^3 w_2 - h_1^3 w_1), \tag{1}$$

where α is the constant ($0 \leqslant \alpha \leqslant 1$) describing the binding between the internal and outer beams. Ignoring the changes in the effective widths, Eq. (1) simplifies as $k^*/k = 1 + \alpha\{(h_2/h_1)^3 - 1\}E_2/E_1$. Using $E_2=70$ GPa for SiO_2 and $E_1=150$ GPa for Si, the coefficient is determined as $\alpha=0.85$ for tip 1 and $\alpha=0.74$ for tip 2.

The changes in the quality factor are analyzed using the Sader formula $k=0.1906wL^2\rho_f Q_f \Gamma_i(\mathrm{Re})\omega_f^2$, where ρ_f is the density of the medium and $\Gamma_i(\mathrm{Re})$ is the hydrodynamic function. The Reynolds number is $\mathrm{Re}=\rho\omega w^2/4\eta$, where $\eta=1.86\times10^{-5}$ kg/m s is the specific viscosity of air. Hence, the Q factor after deposition Q_f^* is

$$Q_f^* = Q_f \frac{k^*}{k} \frac{w\Gamma_i(\mathrm{Re})}{w^*\Gamma_i(\mathrm{Re}^*)} \left(\frac{\omega_f}{\omega_f^*}\right)^2. \tag{2}$$

From Eq. (2) and ignoring the change in Re, the effective Q factor of tip 1 is predicted as 343.1 (vs 335.6, experimental) and tip 2 as 233.7 (vs 244, experimental). Hence, the change in the Q factor is primarily due to the change in the spring

TABLE I. Cantilever properties before and after deposition.

Tip	Sum (V)	Resonance (kHz)	Q	k (N/m)	InvOLS (nm/V)
Tip 1 before	4.14	97.76	288	9.82	95.43
Tip 1 after	4.25	103.10	335.6	13.42	87.78
Tip 2 before	5.61	66.74	156	1.78	75.75
Tip 2 after	5.49	76.14	244.2	3.59	79.72

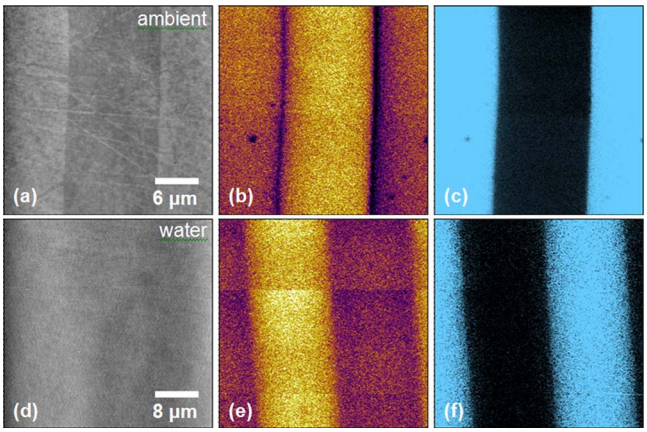

FIG. 3. (Color online) (a) Topography, (b) PFM amplitude, and (c) PFM phase images of PPLN measured with tip 1. The vertical scales are 5 nm for (a) and 10 V for (c). [(d)–(f)] Topography, PFM amplitude, and PFM phase images of PPLN measured with tip 1 in de-ionized water. The vertical scales are 6 nm for (d) and 5 V for (f).

constant and resonance frequency due to the increase in beam thickness, while the increase in the internal damping in the compound beam is smaller than the extrinsic ambient damping.

To characterize the tip geometry, the tip was used to image a calibration grating (TGT01, MikroMasch) containing an array of sharp tips. The blind reconstruction of the tip geometry was performed using the SPIP "tip characterization" option (Image Metrology). Tip 1 (repaired) [Fig. 1(i)] was found to have a 104 nm radius (9.5 nm x radius and 8.7 nm y radius) and cone angles of 35° and 42° along the x and y axis, respectively. The resulting geometry, including the asperity and the surrounding oxide, are clearly visible in Fig. 2(d).

The electrical properties of the conductive tip were probed using I-V measurements in contact with a gold surface (gold-coated mica substrates, Agilent Technologies). The resulting I-V curve [Fig. 2(b)] shows semiconductorlike characteristics and strong asymmetry that can be ascribed both to the semiconducting nature of the tungsten plug and to the Si–W contact. On the reverse bias, the current was found to follow a Schottky-like dependence, $\ln I = a + bV$, where $a = -10.149 \pm 0.001$ and $b = -0.245 \pm 310^{-4}$ and I is in nanoampere. The I-V curve analysis does not allow a description by simple semiconductor models, indicative of the complex character of transport in heavily doped nanoscale contacts.

To test the suitability of the probes for electrical measurements, they were utilized to measure the local electromechanical response of the ferroelectric samples, a method which requires good electrical contact between the tip and the sample. Topography, PFM amplitude, and PFM phase images of PPLN obtained with tip 1 are shown in Figs. 3(a)–3(c), respectively. As expected, the PFM phase provides a strong polarization-dependent contrast. The PFM amplitude image shows nonzero response from both domains. Similar images are obtained in liquid [Figs. 3(d)–3(f)]. While the asymmetry in the magnitude of the response is indicative of some electrostatic component to the signal, the electromechanical contrast is clear, suggesting that there is good electrical contact between the tip and the sample. At this time, the resolution in solution is degraded compared to ambient, and we are now developing probes with improved geometries to maximize spatial resolution. Note that after measuring force-distance curves and several contact mode scans, the tips became mechanically worn, as shown in Figs. 1(g) and 1(h). Note that a broken tip [Fig. 1(g)] can be repaired by using FIB to reopen the via, followed by another EBID fill [Fig. 1(i)].

To summarize, we have developed a process for the fabrication of insulated probes for electrical and electromechanical imaging in liquids and determined the effect of the coating on the dynamic properties of the cantilever. The probe geometry, conductivity, and applicability for electromechanical imaging are illustrated. The EBID process allows easy variation of the probe geometry and composition, allowing for tunable properties. The use of shielded probes may allow precise control over the application and measurement of local fields in solution.

A portion of this research was conducted at the Center for Nanophase Materials Sciences, which is sponsored at Oak Ridge National Laboratory by the Division of Scientific User Facilities, U.S. Department of Energy. P.D.R. gratefully acknowledges support for the Joint Directed Research Development program at UT. One of the authors (S.J.) acknowledges support of the Division of Materials Sciences and Engineering through the Office of Basic Energy Sciences, U.S. Department of Energy at ORNL managed and operated by UT-Battelle, LLC.

[1] R. Plonsey and R. C. Barr, *Bioelectricity: A Quantitative Approach* (Kluwer, New York, 2000).
[2] R. M. Raphael, A. S. Popel, and W. E. Brownell, Biophys. J. **78**, 2844 (2000).
[3] M. C. Liberman, J. Gao, D. Z. Z. He, X. Wu, S. Jia, and J. Zuo, Nature (London) **419**, 300 (2002).
[4] B. J. Rodriguez, S. Jesse, A. P. Baddorf, and S. V. Kalinin, Phys. Rev. Lett. **96**, 237602 (2006).
[5] B. P. Lynch, A. M. Hilton, and G. J. Simpson, Biophys. J. **91**, 2678 (2006).
[6] B. J. Rodriguez, S. Jesse, A. P. Baddorf, S. H. Kim, and S. V. Kalinin, Phys. Rev. Lett. **98**, 247603 (2007).
[7] T. J. Smith and K. Stephenson, in *Scanning Probe Microscopy: Electrical and Electromechanical Phenomena on the Nanoscale*, edited by S. V. Kalinin and A. Gruverman (Springer, New York, 2006), Vol. 1, p. 280.
[8] B. T. Rosner and D. W. van der Weide, Rev. Sci. Instrum. **73**, 2505 (2000).
[9] P. L. T. M. Frederix, M. R. Gullo, T. Akiyama, A. Tonin, N. F. de Rooij, U. Staufer, and A. Engel, Nanotechnology **16**, 997 (2005).
[10] S. J. Randolph, J. D. Fowlkes, and P. D. Rack, Crit. Rev. Solid State Mater. Sci. **31**, 55 (2006).
[11] H. W. P. Koops, R. Weiei, D. P. Kern, and T. H. Baum, J. Vac. Sci. Technol. B **6**, 477 (1988).
[12] A. Gruverman and A. L. Kholkin, Rep. Prog. Phys. **69**, 2443 (2006).
[13] J. E. Sader, J. W. M. Chon, and P. Mulvaney, Rev. Sci. Instrum. **70**, 3967 (1999).
[14] C. P. Green, H. Lioe, J. P. Cleveland, R. Proksch, P. Mulvaney, and J. E. Sader, Rev. Sci. Instrum. **75**, 1988 (2004).
[15] M. J. Higgins, R. Proksch, J. E. Sader, M. Polcik, S. Mc Endoo, J. P. Cleveland, and S. P. Jarvis, Rev. Sci. Instrum. **77**, 013701 (2006).
[16] U. Rabe, K. Janser, and W. Arnold, Rev. Sci. Instrum. **67**, 3281 (1996).
[17] J. A. Turner, S. Hirsekorn, U. Rabe, and W. Arnold, J. Appl. Phys. **82**, 966 (1997).
[18] S. Hirsekorn, U. Rabe, and W. Arnold, Nanotechnology **8**, 57 (1997).